Charley Flach[1]
Fosca Conti[1,2,*]
Ahmet Bayraktar[1]
Markus Goldbrunner[1,*]

Supporting Information available online

Direct Methanation and Storage Concepts for the Flexibilization of Biogas Plants

Enrichment of the methane fraction in a biogas mixture is an innovative possibility to make existing biogas plants more flexible by using excess power. In the described concept, the CO_2 in the biogas is directly catalytically converted into CH_4 with H_2. The CH_4-enriched biogas is again fed into the digester to save energy for later use in the combined heat-and-power unit. Additionally, the fed heat gas can mix and heat the substrate. A heat pipe injector system was therefore developed for cooling the hot biogas stream after methanation and to prevent damage to the microbial consortia during the biomass mixing. The concept was proven at a laboratory-scale biogas plant.

1 Introduction

Power generation from combinations of renewable energy sources like wind, sun, and biomass is the subject of numerous ongoing projects. The development of hybrid-system architectures to manage wind, solar, and biogas energy minimizes limitations due to availability and reliability [1,2]. Indeed, both wind and sunlight are unpredictable renewable energies, and energy harvesting is necessary, which can be compensated by anaerobic digestion processes in fermenters [3,4]. Analysis of power-to-gas [5] applications indicates substantial cost reductions for electrolysis as well as for carbon dioxide methanation during the recent years [6,7]. The aim is usually to methanize the CO_2 content in the biogas mixture, using hydrogen from electrolysis to enable storage of electricity from wind energy and photovoltaic plants [8]. Methanation is the chemical reaction that converts CO_2 to methane and water through hydrogen: $CO_2 + 4H_2 \rightarrow CH_4 + 2H_2O$. A catalyst is necessary for this reaction [9]. This chemical process is also strongly exothermic ($\Delta H = -165\,kJ\,mol^{-1}$) [10] and rapidly approaches equilibrium, so that the main challenge is to handle the massive heat release in terms of temperature resistance of the catalyst and heat transfer properties of the reactor. Then again, it is preferred to avoid wasting the generated heat and it is convenient to use it in the global process of fermentation of the biomass to increase the efficiency of the whole anaerobic digestion process.

In biogas plants, CO_2 can be used as a source for methanation after a complete separation procedure, which is quite complex and expensive. Indeed, the standard power-to-gas concept [5] uses existing biogas plants or wastewater treatment plants only as a CO_2 source for methanation; it is accordingly limited to very large biomethane plants with CO_2 separation concepts. In contrast, the process chain would be considerably simplified if the CO_2 fraction were not completely separated for methanation and the biogas or sewage gas were directly catalytically

converted. In this concept, the biogas would be continuously extracted from the digester and the contained CO_2 transformed into methane would increase the proportion of CH_4 in the gas mixture.

Existing biogas plants already store considerable amounts of biogas under the foil roof of the digester. Since the usual gas storage volume of a biogas plant varies greatly, an estimated average value of $1–2\,m^3kWel^{-1}$ can be assumed. However, this value can be doubled if the CO_2 content in the biogas mixture is completely replaced by CH_4 through direct methanation.

The aim of the present study is to flexibilize the operation of biogas plants by minor technical retrofits and without reducing the electricity production. Therefore, the present study deals with the development, evaluation, and initial estimation of a suitable flexibilization concept by methanization of biogas. This concept is investigated at a representative biogas plant with two digester tanks of 400 and 500 L capacity.

2 Flexibilization Concept

The main advantage of the flexibilization concept is its applicability to existing biogas and sewage treatment plants with gas engines, without costly CO_2 separation. For example, excess

[1]Charley Flach,
Prof. Dr. Fosca Conti (ID) https://orcid.org/0000-0003-4424-1474,
Ahmet Bayraktar, Prof. Dr.-Ing. Markus Goldbrunner
(fosca.conti@unipd.it), (markus.goldbrunner@thi.de)
Technische Hochschule Ingolstadt, Institute of new Energy Systems, Esplanade 10, 85049 Ingolstadt, Germany.

[2]Prof. Dr. Fosca Conti (ID) https://orcid.org/0000-0003-4424-1474
University of Padova, Department of Chemical Sciences, via Marzolo 1, 35141 Padova, Italy.

electricity can be converted into CH_4 during the day and stored in the gas storage tanks of biogas plants or in the digestion towers of a wastewater treatment plant (Fig. 1). Thus, flexibilization of biogas plants is possible without a reduction in electricity production and with only minor technical retrofitting.

Biogas consists of approximately 50 % CH_4 and 45 % CO_2. However, only the combustible methane can be used to generate energy in a combined heat-and-power (CHP) unit. The CO_2 portion of biogas cannot be used for power generation; so, the CO_2 is only a "placeholder" in the gas storage [11]. For this reason, biogas is continuously withdrawn from the digester during the day, as visible in Fig. 1. The CO_2 content in the biogas mixture is then converted into CH_4 by adding hydrogen in what is known as the methanation reaction. The required H_2 can be produced, for example, with the surplus electricity from wind energy and solar collectors. The CH_4-enriched biogas is finally returned to the fermenter. Since the methanation reaction is highly exothermic, the recycled biogas has a temperature of ~250 °C. In addition, water vapor is released during methanation. The described process continuously increases the amount of methane in the gas storage volume of the digester. During the night, the methane-enriched biogas can be converted into electricity via a gas engine (Fig. 1a).

The aim of the present study was to prepare a laboratory scaled-down biogas plant for the catalytic direct methanation of biogas with direct steam generation and direct heating of the fermenter. Experimental measurements were developed to test the possibility of simple retrofitting and flexibilization of existing plants. In this context, the enrichment of the CH_4 content in the biogas storage tank was investigated in the form of an endurance test at the laboratory biogas plant. With the heat pipe technology, a technical option was developed for the introduction and cooling of the hot biogas stream with simultaneous heating of the fermenter. Furthermore, a possible mixing of the substrate by the gas introduction was considered.

## 3 Laboratory-Scale Biogas Plant for Endurance Testing

Fig. 2 shows the laboratory biogas plant at the Technische Hochschule Ingolstadt (THI). The laboratory biogas plant was designed as a scale-down prototype, which allows the use of different solid and liquid substrates to generate biogas with high concentrations of CH_4. The laboratory setup consists of eight main tanks, which are equipped with appropriate agitators for homogeneous mixing of the substrates [12–14]. With the help of a gas analysis system, the gas production of the biogas plant, and thus the efficiency of the used substrates, can be examined. In the Supporting Information, the individual components of the biogas plant are explained in detail together with Fig. S1.

4 Heat Pipe Injector System: Function and Design

At full conversion, the product biogas consists of ~50 % CH_4 and ~50 % H_2O vapor. Direct injection of this mixture into the digester not only utilizes the sensible heat of the gas, but also the condensation heat of the water vapor. This combination significantly increases the efficiency of the process chain. In addition, the direct introduction of the product gas can be used for mixing the substrate: The rising gas bubbles of the product gas can mix the biomass to such an extent that auxiliary energy for operating the electric agitator is not necessary and can be saved. Due to the high temperature (~250 °C) that results after the exothermic methanation process, the microbial consortia in the substrate would be damaged upon contact with the gas flow. Therefore, the gas stream must first be cooled down to nearly the fermenter temperature before blowing it into the bioreactor. For these purposes, in the current study, a new injector concept based upon the heat pipe technology [15, 16] was investigated and an innovative injector system was developed, which utilizes the energy of the product gas for mixing of the substrate and at the same time protects the microorganisms from thermal damage.

For recirculating the hot product gas of the methanation reactor into the biogas digester, the injector concept based on the heat pipe technology was favored. A heat pipe is a closed cylindrical container filled with a working fluid (here: distilled water). The working fluid is in a saturation state between liquid and vapor phase. The inside of the container is characterized by a capillary structure. When one side of the heat pipe is heated, the working fluid evaporates and the vapor flows to the cold end of the pipe, where it condenses and flows
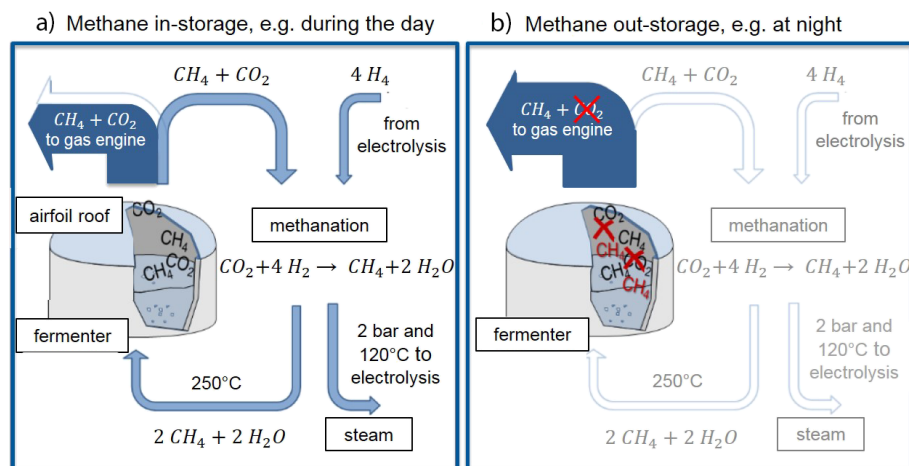
Figure 1. Principle of energy storage through direct methanation of the CO_2 fraction in a biogas mixture. CO_2 in the gas storage tank of the digester is gradually replaced by CH_4 when electricity demand is low.

Figure 2. Scaled-down biogas plant in the biogas laboratory of the THI consisting of (A) slurry storage, (B) water tank, (C) fermentation residue tank, (D) bioreactor 1, (E) bioreactor 2, (F) pre-storage tank for liquids, (G) pre-storage tank for mixed substrate, (H) screw conveyor for automatic feeding, (I) pre-storage tank for solids, and (J) the water filter system. (a) Entire biogas plant and details of (b) the left and (c) the right part of the biogas plant. Red cycles indicate the cast housing of the GRP filters.

5 Determination of the Geometrical Characteristics (Length) of the Heat Pipe

In order to develop the heat pipe, it is necessary to determine the geometric parameters. Overall, the length and diameter of the heat pipe must be adjusted in such a way that the necessary heat flow $\dot{Q}$ can be extracted from the product gas in order to achieve an inlet temperature of 60 °C for the product gas flowing into the fermenter. In a first step, the outer diameter of the heat pipe was determined, and from this information the length of the heat pipe was calculated. The outer diameter of the heat pipe is determined at d_{out} = 30 mm, as noted above and shown in Fig. 3b. First, the evaporator side of the heat pipe ($\dot{Q}$ of the product gas to heat the pipe outer wall) is considered and its length is determined. Then the condenser side ($\dot{Q}$ from the heat pipe to the substrate liquid) is considered and the corresponding length is also calculated. To determine the heat quantity, numerical data related to the product gas are necessary, which are listed in Tab. 1.

Using the parameters of Tab. 1, the energy was calculated via the volume flow rate. Consequently, the corresponding mass flow of the product gas was 9.55×10^{-5} kg s^{-1}. Assuming that no work is done by the product gas, the heat to be transferred can be determined using the first law of thermodynamics (Eq. (1)):

$$\dot{Q} = \dot{m}_{product\ gas} \left[H_{product\ gas}(T_{in}) - H_{product\ gas}(T_{out}) \right] \tag{1}$$

where $\dot{m}_{product\ gas}$ corresponds to the mass flow and $H_{product\ gas}$ corresponds to the temperature-specific enthalpy of the product gas. Including the characteristics of the gas (Tab. 1), for a temperature difference of ΔT = 190 °C, the heat flux to be trans-

back again due to the suction effect of the capillary structure. The idea is to use heat pipe technology to develop a design that enables the use of the heat of the gas flow (product gas) to heat the fermenter and, at the same time, to cool the gas, in order to avoid any damage to the temperature-sensitive microorganisms [17]. In addition, a gas recirculation design is used to mix the biomass in the fermenter. The constructive installation and the developed structure of the heat pipe injector system are shown in Fig. 3.

The main component of the heat pipe injector is the heat pipe itself. The diameter was fixed at 30 mm to allow easy installation in the fermenter wall. The length of the heat pipe (calculations in the following text) was determined by the necessary heat flow $\dot{Q}$ that must be extracted from the product gas in order to achieve an inlet temperature of 60 °C of the gas flowing into the fermenter. The heat pipe injector is installed in the digester wall at an angle of 60° (Fig. 3a). Here, a cable gland is welded into the fermenter wall. Due to the inclined installation at 60°, a higher performance of the heat pipe is realized, because gravity support enables a better backflow of the working medium.

Table 1. Input parameters for the determination of the heat pipe geometry.

Parameter	Value
Volume flow rate of the product gas, $\dot{V}$ [L min^{-1}]	7.12
Input temperature of the product gas, T_{in} [°C]	250
Outlet temperature of the product gas, T_{out} [°C]	60
Total heat flux to be transmitted, $\dot{Q}$ [W]	155
Pressure of the product gas, P [bar]	5.5
H_2 mole fraction in the product gas, xH_2	0.02
CO_2 mole fraction in the product gas, xCO_2	0.04
CH_4 mole fraction in the product gas, xCH_4	0.42
H_2O mole fraction in the product gas, xH_2O	0.52
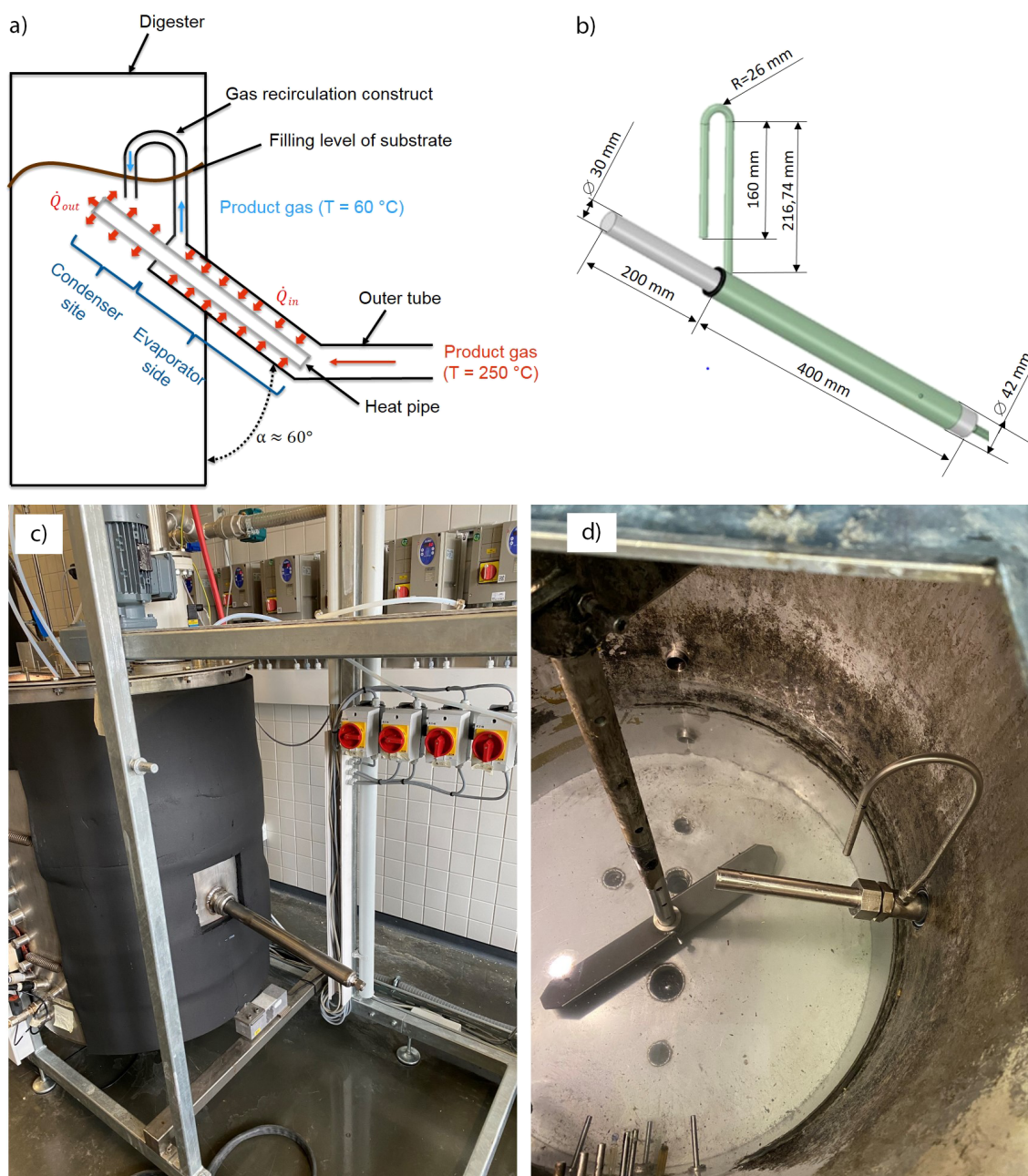
Figure 3. Developed structure of the heat pipe injector system: (a) schematic illustration, (b) geometrical parameters, (c, d) experimental heat pipe injector at the biogas laboratory of the THI: (c) outside and (d) inside components at the bioreactor 2 (element E in Fig. 2a, b).

ferred is 155 W. Assuming that the heat is transferred completely radially to the heat pipe wall (perfect insulation to the environment), this is also the heat that is adsorbed by the heat pipe and transferred to the substrate liquid.

The length of the evaporator side to be calculated can be determined using Eq. (2), which represents an analogy between Ohm's law and thermodynamics [15, 16].

$$\dot{Q} = \frac{\Delta T}{R_{\text{total,EV}}} \qquad (2)$$

In Eq. (2), $R_{\text{total,EV}}$ corresponds to the total thermal resistance of the evaporator side. Due to different heat transfer phenomena occurring, i.e. sensible and latent heat transfer with different heat transfer coefficients, Eq. (2) cannot be used to determine the total thermal resistance for the evaporator side. Instead, the individual heat transfer phenomena with their corresponding heat fluxes and heat transfer coefficients must be determined in order to calculate the individual resistance for each individual heat transfer process. For this purpose, Eq. (2) can be divided into three sections

according to the individual heat transfer phenomena occurring:

$$\dot{Q} = \sum_{i=1}^{j=3} \dot{Q}_i = \sum_{i=1}^{j=3} \frac{\Delta T_{\log,i}}{R_{\text{total,EV},i}} \tag{3}$$

In Eq. (3), $\dot{Q}_i$ corresponds to the heat flux to be transferred, $\Delta T_{\log,i}$ corresponds to the logarithmic temperature difference, and $R_{\text{total},i}$ corresponds to the total thermal resistance in section i. Fig. 4 illustrates the three sections of the heat pipe, the corresponding temperatures, and the calculated heat flow to be transferred.
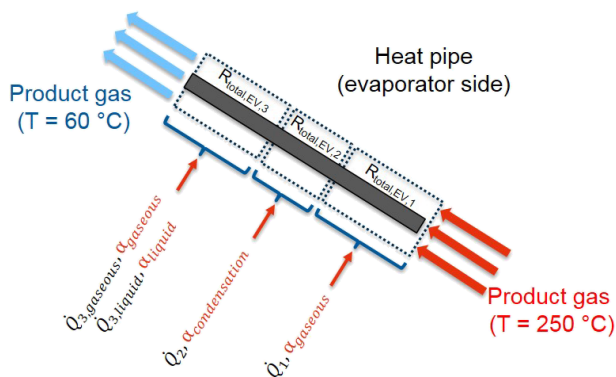
Figure 4. Schematic representation of the heat transfer process in the evaporator side of the developed heat pipe and heat flow parameters, $\dot{Q}_j$.

As can be seen in Fig. 4, the product gas initially transfers $\dot{Q}_1 = 25$ W sensitively to the evaporator wall at an average logarithmic temperature difference of 132 K until the condensation temperature of the water vapor is reached. Subsequently, condensation of the water (latent heat transfer) occurs, transferring $\dot{Q}_2 = 108$ W at a logarithmic temperature difference of 82 K. Finally, the residual heat flows of the product gas of $\dot{Q}_{3,\text{gaseous}} = 7$ W and of the condensate of $\dot{Q}_{3,\text{liquid}} = 15$ W are transferred via convection at a temperature difference of 34 K. The values for $\dot{Q}_1$, $\dot{Q}_{3,\text{liquid}}$, and $\dot{Q}_{3,\text{gaseous}}$ are obtained from Eq. (1) with their respective mass flows of $\dot{m}_1 = 9.55 \times 10^{-5}$ kg s^{-1}, $\dot{m}_{3,\text{gaseous}} = 4.55 \times 10^{-5}$ kg s^{-1}, and $\dot{m}_{3,\text{liquid}} = 5 \times 10^{-5}$ kg s^{-1}, whereas $\dot{Q}_2$ is obtained from the heat of condensation of the water vapor at a condensation temperature of $T_{\text{cond,Water}} = 132\,°C$.

The necessary information about the geometry (length) is contained in the total thermal resistance $R_{\text{total EV},i}$ for the evaporator side and can be described as in Eq. (4).

$$R_{\text{total EV},i} = R_{\text{in,EV},i} + R_{\text{out,EV},i} \tag{4}$$

$R_{\text{in,EV}}$ corresponds to the inner thermal resistance on the evaporator side. $R_{\text{in,EV}}$ results from the radial thermal resistance of the evaporator wall $R_{\text{Wall,EV}}$ and the radial thermal resistance of the capillary structure of the evaporator side $R_{\text{capillary,EV}}$, as reported in Eq. (5).

$$R_{\text{in,EV}} = R_{\text{Wall,EV},i} + R_{\text{c,EV},i} \tag{5}$$

The radial resistance of the evaporator wall $R_{\text{Wall,EV}}$ is described by Fourier's law for circular cylindrical heat pipes as in Eq. (6).

$$R_{\text{Wall,EV},i} = \frac{\ln(d_{\text{out}}/d_{\text{in}})}{2\pi l_{\text{EV},i}\lambda_{\text{Wall}}} \tag{6}$$

In Eq. (6), d_{in} corresponds to the inner diameter of the heat pipe wall and λ_{Wall} corresponds to the thermal conductivity of the wall material. The resistance $R_{\text{capillary,EV},i}$ is calculated in Eq. (7) analogously to Eq. (6).

$$R_{\text{Wall,EV},i} = \frac{\ln(d_{\text{c,out}}/d_{\text{c,in}})}{2\pi l_{\text{EV},i}\lambda_{\text{eff}}} \tag{7}$$

In Eq. (7), $d_{\text{c,out}}$ and $d_{\text{c,in}}$ are the outer and inner diameter of the capillary structure, respectively. λ_{eff} corresponds to the effective thermal conductivity of the capillary structure. According to [16], the following expression is obtained for λ_{eff} in the case of sintered structures, which are used in the current study:

$$\lambda_{\text{eff}} = \frac{\lambda_l[(2\lambda_{\text{medium}} + \lambda_{\text{Wall}}) - 2(1-\varepsilon)(\lambda_{\text{medium}} - \lambda_{\text{Wall}})]}{(2\lambda_{\text{medium}} + \lambda_{\text{Wall}}) + (1-\varepsilon)(\lambda_{\text{medium}} - \lambda_{\text{Wall}})} \tag{8}$$

In Eq. (8), λ_{medium} corresponds to the thermal conductivity of the working medium (water), and ε, to the porosity of the capillary structure.

Of particular interest for heat transfer, however, is the radial resistance between the outer heat source and the evaporator wall, $R_{\text{out,EV},i}$. The outer thermal resistances on the evaporator side, on the other hand, are dependent on convective processes as well as the phase change (condensation) of the water vapor and can be generally determined with Eq. (9).

$$R_{\text{out,EV},i} = \frac{1}{\alpha_i A_{\text{out},i}} = \frac{1}{\alpha_i 2\pi l_{\text{EV},i} d_{\text{out}}} \tag{9}$$

In Eq. (9), α_i is the sectional heat transfer coefficient between the product gas and the evaporator wall, $A_{\text{out},i}$ is the outer surface area, and $l_{\text{out},i}$ is the length of the corresponding evaporator section of the heat pipe in the respective section i. In the case of convective heat transfer, it is useful to correlate coefficient α_i to the Nusselt number Nu_i, which is the ratio of convective to conductive heat transfer across a boundary. Therefore, α_i in convective heat transfer is a function of Nu_i, as described in Eq. (10).

$$\alpha_i = \frac{Nu_i \lambda_i}{d_{\text{out}}} \tag{10}$$

Under the assumption that the fluid is supposed to transfer heat in a "pipe-to-pipe" construct (see Fig. 3a), Nu correlations of cylindrical pipe flows can be used. Here, the assumption is that the heat is transferred exclusively radially into the heat pipe wall and that perfect insulation to the outside is the case. For flow in a cylindrical pipe, experimental observations show that laminar flow occurs when the Reynolds number Re is less than 2300, and turbulent flow occurs when $Re > 2900$. For forced convection in laminar pipe flow, Nu can be expressed as a function of Re and of the Prandtl number (Pr). The following correlation was used in the present study [18]:

$$Nu_i = \sqrt[3]{3.66^3 + 0.644^3 Pr \left(Re_i \frac{d_{out}}{l_{EV,i}} \right)^{3/2}} \qquad (11)$$

Since $l_{EV,i}$ is the quantity to be determined, Nu as well as the heat transfer coefficient are determined iteratively by specifying an initial value of $l_{EV,i} = 0.3$ m.

Sensible heat transfer is followed by latent heat transfer due to condensation of the water vapor in the product gas mixture. Here, the latent heat of the vapor is introduced to the evaporator wall of the heat pipe. To determine the heat transfer, Nusselt's water skin theory (film condensation) can be used in a first step. This determines an average heat transfer coefficient for the entire condensation process. For the condensation of the water vapor on the evaporator surface of the heat pipe, the heat transfer coefficient α_{cond} for a circular cylinder can be used as an approximation [19].

$$\alpha_{cond} = 0.728 \left(\frac{\rho_l(\rho_l - \rho_v)g\Delta H_{cond}\lambda_l^3}{\eta_l(T_S - T_{Wall})} \frac{1}{d_{out}} \right) \qquad (12)$$

In Eq. (12), ρ_l is the density of the liquid phase, ρ_v is the density of the vapor, ΔH_{cond} is the enthalpy of condensation, η_l is the dynamic viscosity of the liquid phase, λ_l is the thermal conductivity of the liquid phase, T_S is the saturation temperature of the water, and T_{Wall} is the wall temperature of the heat pipe.

In analogy to the calculation of the length of the evaporator side, the length of the condenser side can be determined using Eq. (4). Since the heat transfer from the heat pipe outer wall to the substrate liquid takes place here and the only outer heat transfer mechanism is through free convection, the entire length of the condenser side can be calculated with a single heat transfer coefficient. A sectional determination of the geometry length as with the evaporator side does not take place. The Nusselt number for free convection, Nu_{FC}, can be determined as in Eq. (13).

$$Nu_{FC} = \left(0.752 + 0.387 Ra^{1/6} f_3(Pr) \right)^2 \qquad (13)$$

Here, Ra corresponds to the Rayleigh number and f_3 to a correction factor of the Prandtl number.

Using Eq. (10), the heat transfer coefficient for free convection α_{FC} is determined and Eq. (5) is used to determine the length of the condenser side. The calculated results for the evaporator side and condenser side of the heat pipe can be seen in Tab. 2.

The resulting total lengths of the components are only estimates since average heat transfer rates were used. To accommodate these inaccuracies in the design and installation, the final length for the evaporator side was increased to 0.4 m, and of the condenser side, to 0.2 m (see detailed 3D sketch in Fig. 3b). Thus, further investigations are planned for a more accurate determination of the heat transfer and the corresponding lengths.

6   Particle Filter System

Particles can be transported through the fluid flow and are eventually deposited as a layer of solid particles on the bed or

Table 2. Calculated output parameters α_i and l_i.

Heat transfer coefficient α_i [W m^{-2}K^{-1}]	Length l_i [m]
24 ($\alpha_{1,gaseous,convective}$)	
17 219 ($\alpha_{2,condensation}$)	
23 ($\alpha_{3,gaseous,convective}$)	0.19 (evaporator side)
311 ($\alpha_{4,liquid,convective}$)	
728 (α_{FC})	0.13 (condenser side)

bottom of a body. In a gas system, these particles can be rust flakes from the water lines, small pieces of organic matter, sand grains, clay particles, or other small particles from the water supply. If the particles are in the gas stream, they can cause significant malfunctions or can even damage sensitive components in the test operation. For example, particles in the gas can cause problems with gas meters, solenoid valves, or the mass flow controller. Particle deposits can lead to inaccurate measurements or even the destruction of some components. In addition, the methanation reactor is particularly sensitive to solid particles in the gas, as these would be deposited in the catalyst bed. The catalyst bed is the heart of the methanation reactor and is flowed through by the biogas. The chemical catalyst is nickel, which is in the form of a coating of many small cylindrical pellets made of the carrier material Al_2O_3. The pellets have a diameter of 2 mm and a length of 4 mm. Since the conversion of CO_2 and H_2 to CH_4 takes place on the surface of the coated pellets, there is an increased pressure loss during methanation and a loss of the active surface of the catalyst. In the worst case, this can lead to the deactivation of the catalyst.

In order to remove the unwanted solid particles from the biogas, a two-stage water filter system was developed (see element "J" in Fig. 2). The system is composed of two tanks, with identical design. Each tank has a capacity of 38 L and a cylindrical form with a screw-off lid, a rubber sealing layer, and an inlet pipe to flow the biogas obtained in the laboratory plant. The inlet pipe has a length of 20 cm and a diameter of 1 cm. Both tanks were made of a 2-mm-thick stainless-steel sheet to ensure a long service life. Fig. 5 shows the design of one tank of
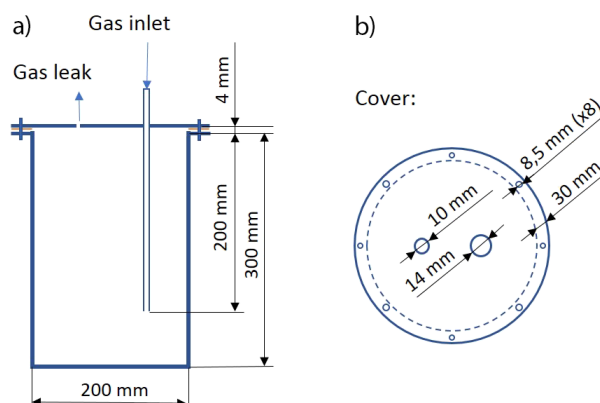
Figure 5. Schematic illustration with experimental dimensions of one tank of the two-stage water filter: (a) side view, (b) top view.

the developed two-stage water filter and the geometric dimensions.

6.1 Fine Particles in the Biogas Stream

To determine the amount of fine particles in the biogas stream, the biogas was analyzed directly after leaving bioreactor 2. For this purpose, a filter combination consisting of a glass fiber-reinforced plastic (GRP) mat and a paper filter was placed in the GRP filter cast housing attached to the digester outlet.

The biogas first flows through the GRP filter mat, so that all particles with a size of above $50 \, \mu m$ can be filtered out from the biogas. Since the paper filter is placed above the filter mat, it can filter out all particles with sizes between 50 and $10 \, \mu m$. Particles with cross-sectional diameter smaller than $10 \, \mu m$ are thus not filtered. This aspect is taken into account during the evaluation. Details are reported in the Supporting Information together with Fig. S2.

The evaluation showed that most of the particles were deposited between the filter mat and the coffee filter. This suggests that most of the particles contained in the biogas have a particle size between 10 and $50 \, \mu m$. Larger and therefore heavier particles were sighted in the fabric of the GRP filter mat. In total, a mass of 1.233 g of solid particles in the biogas was determined using this method over a period of 2 weeks. This mass is defined as the total mass of particles in the biogas.

6.2 Determination of Solid Particles in Water Filters

The second series of experiments was intended to investigate the operation of the two-stage water filter. The aim was to determine the mass of particles deposited per filter stage and thus filtered out of the biogas. For this purpose, all the biogas produced by the laboratory plant was passed directly through the water filters. During the procedure, the GRP filter was deactivated, i.e. no pre-filtering was included in the process setup.

After the experimental period, the filters were removed from the system and the mass of solids in each filter stage was measured after a period of 2 days in the oven at a temperature of $80 \, °C$ for drying.

The developed two-stage water filter system was able to filter out a total of 1.217 g of foreign particles from the biogas. Of these, 1.123 g of particles was filtered out of the biogas with the first filter stage and 0.094 g of particles was filtered out with the second filter stage. In terms of the total mass of fine particles removed with the water filter, approximately 92 % of the particles were filtered out with the first filter stage and approximately 8 % of the particles were filtered out with the second filter stage. In conclusion, although the majority of the particles were extracted with the first filter stage, the second stage was an important component. In relation to the total mass of fine particles contained in the biogas, the water filter system showed an overall efficiency of 98.7 %. Finally, it was observed that the gas lines after the water filter were no longer contaminated, in contrast to the lines before the water filter. Accordingly, it is concluded that the fraction of particles with size smaller than $10 \, \mu m$ in the biogas is very low.

7 Conclusions

The CH_4 storage system of a laboratory scaled-down biogas plant was designed and investigated. The plant consists of pre-storage tanks for solids, liquid, and slurry, two bioreactors with capacities of 400 and 500 L, a fermentation residual tank, and a water tank to optimize the consistency of the biomass for the final disposal. To automatically feed the two bioreactors, a screw conveyor with a diameter of 10 cm was added.

By in situ direct conversion of CO_2 to CH_4 via nickel catalysis and hydrogen addition, a methanation process was planned to enrich the gas mixture and increase the efficiency and flexibility of the plant. The power-to-gas concept was integrated by the flexbiomethane concept, where the CO_2 in the produced biogas mixture is temporarily stored in the existing gas storage volume of the fermenter.

A heat pipe injector system was developed to blow the produced biogas from the first fermentation process into the second bioreactor. The recirculated gas flow was selected to mix the biomass, and a special design of the injector was investigated to achieve this aim. The optimization of the heat pipe geometry suggests using an angle of 60° for the installation and a pipe with a diameter of 3 cm. The mass flow of the product gas was estimated to be $\sim 10^{-4} \, kg \, s^{-1}$ with a temperature difference of 190 °C between the two positions where the heat flux is to be transferred. It turns out that the heat flux to be transferred is $\sim 155 \, W$ between the two heat side positions at the temperatures of 250 and 60 °C, respectively. The length of the evaporator side for gaseous and liquid convection and condensation was calculated to be 19 cm, while the length of the condenser side for free convection was found to be 13 cm.

Unwanted solid particles were found along the gas line. Therefore, a fine-particle filter system was implemented. A water system with two separated tanks with a capacity of $\sim 40 \, L$ was developed. A total of 1.2 g of dried solid particles was collected after a test period of 2 weeks. Of this, 92 % was collected in the first filter stage. In addition to the water two-stage system, a plastic filter based on a glass fiber mat was developed. The gas line contamination by the solid particles from the biogas was successfully eliminated by the ideated filter system.

Finally, computational fluid dynamics simulations are planned to investigate flow and heat transfer with the aim to set a model and validate it with the experimental results.

Supporting Information

Supporting Information for this article can be found under DOI: https://doi.org/10.1002/ceat.202200239.

Acknowledgments

The authors have declared no conflict of interest.

Symbols used

A	[mm^2]	surface area
d	[mm]	diameter
f	[–]	correction factor of the Prandtl number
g	[m s^{-2}]	acceleration factor due to gravity
H	[J]	enthalpy
l	[mm]	length
$\dot{m}$	[kg s^{-1}]	mass flow
Nu	[–]	Nusselt number
P	[bar]	pressure
Pr	[–]	Prandtl number
$\dot{Q}$	[W]	heat flow
R	[K W^{-1}]	thermal resistance
Ra	[–]	Rayleigh number
Re	[–]	Reynolds number
T	[°C]	temperature
$\dot{V}$	[L min^{-1}]	volume flow rate
x	[–]	mole fraction

Greek symbols

α	[W m^{-2}K^{-1}]	heat transfer coefficient
ε	[–]	porosity
η	[kg m^{-1}s^{-1}]	dynamic viscosity
λ	[W m^{-1}K^{-1}]	thermal conductivity
ρ	[kg m^{-3}]	density

Subscripts

c	capillary
cond	condensed
eff	effective
EV	evaporator section
FC	free convection
in	inner
l	liquid
out	outer
S	saturation
v	vapor

Abbreviations

CHP	combined heat-and-power
GRP	glass fiber-reinforced plastic
THI	Technische Hochschule Ingolstadt

References

[1] S. Mishra, C. K. Panigrahi, D. P. Kothari, *Int. J. Ambient Energy* **2016**, *37 (2)*, 184–191. DOI: https://doi.org/10.1080/01430750.2014.915886

[2] K. Singh, H. Singh, *Int. J. Res. Educ. Methodol.* **2015**, *7 (4)*, 1248–1256. DOI: https://doi.org/10.24297/ijrem.v7i4.4362

[3] P. Malik, M. Awasthi, S. Sinha, *Int. J. Energy Res.* **2021**, *45 (3)*, 3464–3494. DOI: https://doi.org/10.1002/er.6061

[4] Q. Liu, Z. Bai, X. Wang, J. Lei, H. Jin, *Energy Convers. Manage.* **2016**, *122*, 252–262. DOI: https://doi.org/10.1016/j.enconman.2016.05.080

[5] R. Peters, M. Baltruweit, T. Grube, R. C. Samsun, D. Stolten, *J. CO2 Util.* **2019**, *34*, 616–634. DOI: https://doi.org/10.1016/j.jcou.2019.07.009

[6] M. Thema, F. Bauer, M. Sterner, *Renewable Sustainable Energy Rev.* **2019**, *112*, 775–787. DOI: https://doi.org/10.1016/j.rser.2019.06.030

[7] S. O. Babalola, J. J. Nel, V. Tshigo, M. O. Daramola, S. A. Iwarere, *Energy Convers. Manage.* **2022**, *258*, 115551. DOI: https://doi.org/10.1016/j.enconman.2022.115551

[8] J. Daniel-Gromke, V. Denysenko, T. Barchmann, T. Reinelt, M. Trommler, in *Dezentrale Energieversorgung* (Eds: K. J. Thomé-Kozmiensky, M. Beckmann), Thomé-Kozmiensky Verlag, Berlin **2014**, pp. 133–150. ISBN: 978-3-935317-95-5

[9] C. G. Takoudis, *J. Catal.* **1982**, *78 (1)*, 265. DOI: https://doi.org/10.1016/0021-9517(82)90309-8

[10] M. Seemann, H. Thunman, *Substitute Natural Gas from Waste* **2019**, 221–243. DOI: https://doi.org/10.1016/B978-0-12-815554-7.00009-X

[11] V. Di Noto, K. Vezzù, G. A. Giffin, F. Conti, A. Bertucco, *J. Phys. Chem. B* **2011**, *115 (46)*, 13519–13525. DOI: https://doi.org/10.1021/jp207917n

[12] F. Conti, A. Saidi, L. Wiedemann, M. Sonnleitner, M. Goldbrunner, *26th Eur. Biomass Conf. and Exhibition Proc.*, Eta-Florence Renewable Energies, Florence **2018**, pp. 811–815. DOI: https://doi.org/10.5071/26thEUBCE2018-2CV.5.34

[13] F. Conti, L. Wiedemann, A. Saidi, M. Goldbrunner, *IOP Conf. Series: Mater. Sci. Eng.* **2018**, *446*, 012011. DOI: https://doi.org/10.1088/1757-899X/446/1/012011

[14] L. Wiedemann, F. Conti, M. Sonnleitner, A. Saidi, M. Goldbrunner, *25th Eur. Biomass Conf. and Exhibition Proc.*, Eta-Florence Renewable Energies, Florence **2017**, pp. 889–892. DOI: https://doi.org/10.5071/25thEUBCE2017-2CV.4.14

[15] D. Reay, R. McGlen, P. Kew, *Heat Pipes: Theory, Design and Applications*, Elsevier, Amsterdam **2006**. ISBN: 9780080982663

[16] G. P. Peterson, *An Introduction to Heat Pipes: Modeling, Testing, and Applications*, John Wiley & Sons, New York **1994**. ISBN: 9780471305125

[17] M. Trentini, M. Lorenzon, F. Conti, *26th Eur. Biomass Conf. and Exhibition Proc.*, Eta-Florence Renewable Energies, Florence **2018**, pp. 816–820. DOI: https://doi.org/10.5071/26thEUBCE2018-2CV.5.35

[18] P. Böckh, C. Saumweber, *Fluidmechanik. Einführendes Lehrbuch*, Springer, Wiesbaden **2013**. ISBN: 9783642338922

[19] H. D. Baehr, K. Stephan, *Wärme- und Stoffübertragung*, Springer, Wiesbaden **2016**. ISBN: 9783642055003